ACS central science

http://pubs.acs.org/journal/acscii

Research Article

Enantioseparation in Hierarchically Porous Assemblies of Homochiral Cages

Chengfeng Zhu,* Keke Yang,# Hongzhao Wang,# Yu Fang,# Liang Feng, Jiaqi Zhang, Zhifeng Xiao, Xiang Wu, Yougui Li,* Yanming Fu, Wencheng Zhang, Kun-Yu Wang,* and Hong-Cai Zhou*

Cite This: *ACS Cent. Sci.* 2022, 8, 562−570

Read Online

ACCESS | Metrics & More | Article Recommendations | Supporting Information

ABSTRACT: Efficient enantioselective separation using porous materials requires tailored and diverse pore environments to interact with chiral substrates; yet, current cage materials usually feature uniform pores. Herein, we report two porous assemblies, **PCC-60** and **PCC-67**, using isostructural octahedral cages with intrinsic microporous cavities of 1.5 nm. The **PCC-67** adopts a densely packed mode, while the **PCC-60** is a hierarchically porous assembly featuring interconnected 2.4 nm mesopores. Compared with **PCC-67**, the **PCC-60** demonstrates excellent enantioselectivity and recyclability in separating racemic diols and amides. This solid adsorbent **PCC-60** is further utilized as a chiral stationary phase for high-performance liquid chromatography (HPLC), enabling the complete separation of six valuable pharmaceutical intermediates. According to quantitative dynamic experiments, the hierarchical pores facilitate the mass transfer within the superstructure, shortening the equilibrium time for adsorbing chiral substrates. Notably, this hierarchically porous material **PCC-60** indicates remarkably higher enantiomeric excess (ee) values in separating racemates than **PCC-67** with uniform microporous cavities. Control experiments confirm that the presence of mesopores enables the **PCC-60** to separate bulky substrates. These results uncover the traditionally underestimated role of hierarchical porosity in porous-superstructure-based enantioseparation.

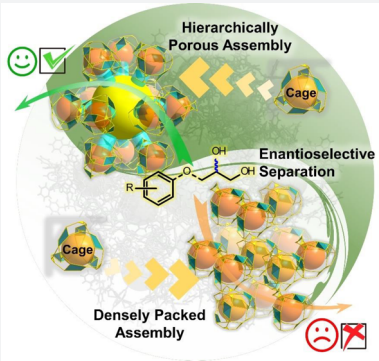

■ INTRODUCTION

Chirality is a crucial factor in the safety and efficacy of drugs. Given that those opposite racemates of many drug molecules are inactive or even toxic, it is always one hotspot in the pharmaceutical industry to produce enantiopure intermediates or drugs.[1−4] Enantioselective separation is an economical and practical method to obtain enantiopure compounds, compared with other techniques such as asymmetric catalysis. Porous materials, including metal−organic frameworks (MOFs) and covalent organic frameworks (COFs), are promising candidates for enantioseparation due to their tailored and diverse pore environments, enabling strong interactions with chiral substrates.[5−14] Porous coordination cages (PCCs) are emerging materials with tunable inherent cavities.[15−21] In particular, incorporating chirality into the PCC will create a unique chiral microenvironment, promoting the selective binding of enantiomers and endowing the material with application potentials in various fields, including enantioselective separation.[22−30] To date, extensive studies have been made to regulate the inherent cavities of chiral PCCs. For instance, Mukherjee and co-workers constructed an enantiopure Pd_{12} tetrahedral nanocage with a large hydrophobic cavity, which showed enantioselectivity to bind racemic 1,1′-binaphthalene-2,2′-diol and 2,2′-diethoxy-1,1′-binaphthalene.[30] Cui and co-workers adopted an enantiopure 1,1′-binaphthyl-diketone-derived ligand to construct a Fe-based tetrahedral cage, enabling resolving racemic 2-butanol and 3-methyl-2-butanol with enantiomeric excess (ee) values up to 99.5%.[31] Su and co-workers assembled homochiral Fe−Pd heterometallic cages to separate atropisomers with the best enantioselectivity of 88% ee.[32] Many such chiral PCCs featured promising capability in enantioseparation. Yet, the high enantioselectivity and the wide substrate scope are often mutually exclusive in state-of-the-art chiral cages for enantioseparation.[33−36] Moreover, most cage-based enantioseparation studies focus on the uniform intrinsic cavities, and the role of extrinsic pores is often underestimated. In nature, enzymes usually feature binding pockets connected with the exterior environment by channels, ensuring the access of substrates to interact with active sites. Taking a page from nature, we presume that hierarchical pores or interconnected mesopores may facilitate the ingress of substrates into porous materials, eliminating adsorption only at the surface. The utilization of multiple pore environments in synergy can, in principle, confer more binding sites and better mass transfer on

Received: December 22, 2021
Published: April 22, 2022

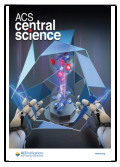

ACS Publications

© 2022 The Authors. Published by American Chemical Society

PCCs. It is challenging, however, to assemble cage units into hierarchical porous superstructures while maintaining their structural integrity and stability.

This work presents a case wherein a homochiral hierarchically porous assembly, **PCC-60**, is constructed with dual-walled octahedral lanthanide coordination cages. The **PCC-60** consists of intrinsic 1.5 nm microporous cavities that are connected by 2.4 nm extrinsic mesopores. As a solid adsorbent, the **PCC-60** demonstrates ee values up to 99.9% in separating various racemic diols and amides, and no loss in performance is observed after five cycles. To confirm its utility in practical separation, the **PCC-60** can directly serve as a chiral stationary phase for HPLC, enabling the complete and efficient separation of six racemates. The **PCC-60**-based HPLC column can separate up to 60.0 μg of racemates with separation efficiencies up to 30 816 plates per meter, representing one of the best porous materials for preparative HPLC. Interestingly, through tuning the synthetic conditions, the coordination cages of **PCC-60** can be crystallized into a densely packing mode to achieve a microporous assembly, **PCC-67**, as a control group for separation studies. According to quantitative dynamic experiments, the hierarchical pores facilitate the mass transfer within the **PCC-60** superstructure, shortening the equilibrium time for adsorbing chiral substrates. Compared to the **PCC-67** with uniform microporous cavities, the hierarchically porous **PCC-60** indicates remarkably higher ee values in enantioseparation. Control experiments also confirm that the presence of mesopore enables the **PCC-60** to separate bulky substrates, demonstrating tolerance toward a wide range of substrates. To the best of our knowledge, this work presents the first example of hierarchically porous superstructures assembled from chiral cages, which uncovers the traditionally underestimated role of hierarchical porosity in porous-superstructure-based enantioseparation.

■ RESULTS AND DISCUSSION

Synthesis, Structure, and Characterization of Cage Compounds. As shown in Scheme 1, the heating of chiral ligand (H_3**L**) derived from L-phenylalanine and $NdCl_3{\cdot}6H_2O$ (1:3 molar ratio) in a DMF−EtOH−H_2O solvent mixture with the addition of formic acid afforded pale-purple hexagonal block crystals of **PCC-60**. Light-yellow parallelogram block crystals of **PCC-67** were obtained under a similar reaction condition when replacing formic acid and $NdCl_3{\cdot}6H_2O$ with propiolic acid and $HoCl_3{\cdot}6H_2O$ (for detailed synthesis, see the Supporting Information). The chemical compositions of **PCC-60** and **PCC-67** can be formulated as $[Nd_{12}\mathbf{L}_8(O_2CH)_{12}{\cdot}24H_2O]$ and $[Ho_{24}\mathbf{L}_{16}(O_2CC{\equiv}CH)_{24}{\cdot}48H_2O]$, respectively, based on the results of single-crystal X-ray analysis, infrared spectroscopy (IR), and thermogravimetric analysis (TGA). Notably, the internal cavities of the cages were decorated with a high density of residues from L-phenylalanine, analogizing the hydrophobic binding pockets of enzyme proteins.[37,38] In addition, **PCC-60** and **PCC-67** are stable for months in common organic solvents, such as methanol, acetonitrile, tetrahydrofuran, dichloromethane, and acetone.

Scheme 1. Construction of the Octahedral Cages of PCC-60 and PCC-67

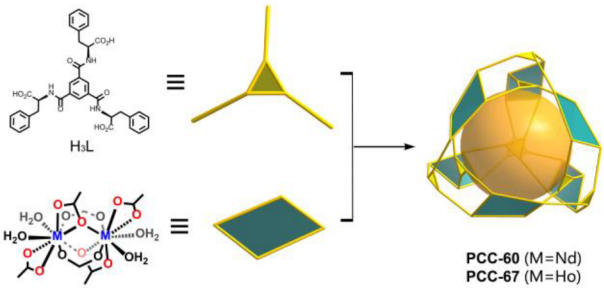

The single-crystal X-ray diffraction studies on **PCC-60** and **PCC-67** demonstrate the formation of rare dual-walled octahedral $Ln_{12}\mathbf{L}_8$-based cages.[39−41] The superstructure **PCC-60** is crystallized in a chiral hexagonal $P6_3$ space group with one formula in the unit cell. The cage is comprised of six crystallographically independent binuclear $Nd_2(CO_2)_6$ clusters serving as vertexes and four pairs of highly flexible **L** ligands as four faces of the octahedron. As such, the cage features a dual-walled topological structure with a 1.5 nm inner chiral cavity and four open trigonal windows in a dimension of 1.3 × 1.3 nm^2. Besides, a spindle-like mesopore with a maximum inner width of 2.4 nm is formed via the orderly arrangement of 12 octahedral cages, directed by intermolecular C−H···π interactions (Figure 1a and Figure S1). In particular, the open windows of coordination cages are oriented toward the extrinsic mesopore, offering interconnected channels to facilitate the mass transfer (Figure 1b).[42,43]

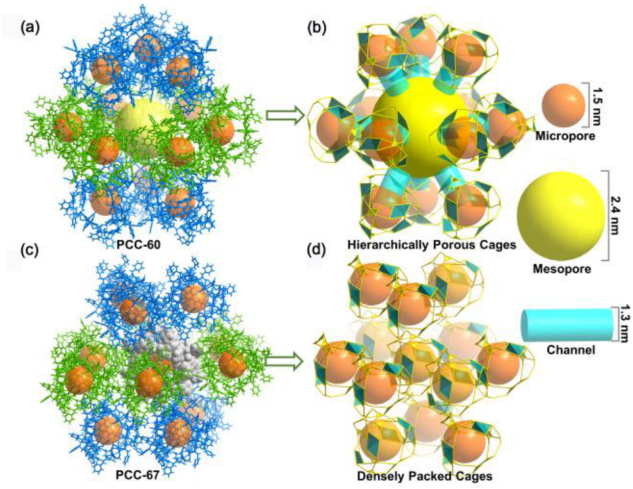

Figure 1. Views of (a) the arrangement of octahedral cages and (b) the hierarchical porous structure in the supramolecular assembly of **PCC-60**; views of (c) the densely packed mode of octahedral cages and (d) microporous structure in **PCC-67**. The orange ball represents the inner cavity, while the yellow ball represents the large external cavity. The gray molecule represents a single octahedral cage surrounded by 12 cages.

PCC-67 is assembled from identical dual-walled octahedral cages as that in **PCC-60**. However, it crystallizes in a chiral triclinic $P1$ space group, and its unit consists of two identical cages, in which the octahedron vertices are replaced by binuclear $Ho_2(CO_2)_6$ clusters. In particular, the superstructure **PCC-67** adopts an arrangement mode significantly different from that in **PCC-60** (Figure 1c). In **PCC-67**, each open window of the octahedral cage, as the potential portal for guest inclusion, is almost blocked by the faces of adjacent cages (Figure 1d and Figure S1). Therefore, narrow channels with a dimension of 0.61 × 0.68 nm and 0.59 × 0.31 nm, respectively, are formed by densely packed cages along the crystallographic

https://doi.org/10.1021/acscentsci.1c01571
ACS Cent. Sci. 2022, 8, 562−570

a axis (Figure S1). Note that the different packing modes of cages can generate various porosity. For instance, Banerjee and co-workers reported a highly stable imine-bonded cage that adopted three polymorphic forms with varied crystallographic packings, leading to a porosity switch between porous and nonporous forms.[44,45]

The powder X-ray diffraction (PXRD) patterns obtained from the bulk samples of **PCC-60** and **PCC-67** demonstrate a slight peak shift compared with ones simulated from corresponding single-crystal structures. The Platon Squeeze was utilized to remove disordered solvent residues in the single-crystal structural refinement, which could change the peak position and sharpness of the simulated PXRD patterns (Figure S2). The IR spectrum shows that the characteristic peak for the carboxyl stretch $\nu_{C=O}$ around 1725 cm^{-1}, which originated from the ligand H_3**L**, disappears in the spectra of **PCC-60** and **PCC-67**, indicating the formation of coordination bonds (Figure S3). TGA analysis shows that the guest solvent molecules in the cage compounds of **PCC-60** and **PCC-67** would be gradually lost as the temperature increased to ca. 220 and 250 °C, respectively (Figure S4). According to the variable-temperature PXRD patterns of **PCC-60**, the cage assembly would be collapsed between 150 and 200 °C. In addition, the circular dichroism (CD) spectra of cages constructed with (*S*)- and (*R*)-enantiomers of the H_3**L** ligand are mirrored versions of each other, demonstrating their enantiomeric nature in crystalline states (Figure S5).

PLATON calculations suggest that approximately 57.7% and 46.1% of the total volume are occupied by guest molecules in **PCC-60** and **PCC-67**, respectively.[46] Besides, the accessible porosity of the two cage-based assemblies were confirmed by dye adsorption in solution. It showed that **PCC-60** could adsorb 3.25 methylene orange (MO, 1.25 nm × 0.50 nm × 0.38 nm in size) per formula unit. However, only surface adsorption of MO was observed for **PCC-67** under identical conditions (Figure S6). This phenomenon should be attributed to the presence of interconnected mesopores in **PCC-60** that enable the inclusion of bulky molecules.

In both **PCC-60** and **PCC-67**, each M_{12}**L**$_8$ (M = Nd or Ho) cage contains a high density of chiral sites from ligands and metal centers. There are 24 uncoordinated chiral amide groups and 12 metal centers in an individual coordination cage with the Δ-configuration exposed to the interstitial spaces. The inherent cavities allow the guest molecules to access these chiral sites. The presence of the sophisticated chiral microenvironment and accessible cavities, therefore, inspired us to study the superstructures' enantioselectivity toward various chiral molecules.

Enantioselective Adsorption and Separation. After the structural details of **PCC-60** and **PCC-67** were obtained, their enantioselective adsorption and separation toward chiral diols, which are valuable pharmaceutical intermediates, were investigated.[47−49] Initially, for the condition optimization, (*S*)-**PCC-60** single crystals were immersed in solutions containing racemic 1-phenylethane-1,2-diol (PED), a model analyte, and different solvents at room temperature (Table 1). The results indicate that acetone was the most suitable solvent for the enantiosorption, giving rise to the (*R*)-enantiomer of PED with 99.6% ee after the extraction (Figure S7). We presumed that the high solubility of chiral PED molecules in acetone might contribute to the removal of racemic PED on the crystal surface and the (*S*)-enantiomer of PED trapped within the chiral cage. When (*R*)-**PCC-60** was used as an adsorbent, the (*S*)-enantiomer of PED with 99.8% ee can be obtained, indicating the chirality of the host superstructures controls the inclusion of racemic diols. In addition, kinetic studies indicated that the adsorption of PED in **PCC-60** could reach equilibrium in around 5 h, generating a host−guest complex with a ratio of about 1:5.2 (**PCC-60**/PED) (Figure S8). Besides, the PED with a moderate ee value can be obtained under the optimized separation condition, when (*S*)-**PCC-67** and (*R*)-**PCC-67** were employed as adsorbents (entries 8 and 9 in Table 1, Figure S7). Presumably, the variety in enantioselectivity between **PCC-60** and **PCC-67** might arise from their different porosities.

Table 1. Enantioselective Separation of Racemic 1-Phenylethane-1,2-diol with PCC-60 and PCC-67

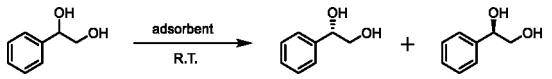

entry	solvent	sorbent	ee (%)[a]
1	THF	(*S*)-**PCC-60**	19.7 (*R*)
2	EtOH	(*S*)-**PCC-60**	47.9 (*R*)
3	CH_3CH	(*S*)-**PCC-60**	57.1 (*R*)
4	CH_2Cl_2	(*S*)-**PCC-60**	71.9 (*R*)
5	MeOH	(*S*)-**PCC-60**	83.9 (*R*)
6	$(CH_3)_2CO$	(*S*)-**PCC-60**	99.6 (*R*)
7	$(CH_3)_2CO$	(*R*)-**PCC-60**	99.8 (*S*)
8	$(CH_3)_2CO$	(*S*)-**PCC-67**	65.0 (*R*)
9	$(CH_3)_2CO$	(*R*)-**PCC-67**	66.1 (*S*)

[a]ee values were obtained by HPLC.

To further understand the contribution of hierarchical porosity to the enantiosorption, we carried out three sets of control enantiosorption experiments of chiral diols using adsorbents **PCC-60** and **PCC-67**.[50−52] Initially, crystals of (*S*)-**PCC-60** or (*S*)-**PCC-67** (with the same molar cages of ca. 2.0 μmol) were soaked in 2 mL of acetone containing 20 μmol of racemic diols. Then, the chiral diols in the supernatant were monitored by HPLC in terms of the peak area and ee value (Figure S9). As shown in Figure 2b, the total peak areas of PED dramatically decreased from ∼6643 ± 73 to ∼3011 ± 38 when (*S*)-**PCC-60** was employed as the adsorbent after 5 h, providing a ∼53% ee of PED with (*S*)-enantiomer in excess. This result implies that ∼54% of total PED molecules can be encapsulated by (*S*)-**PCC-60**, with (*R*)-enantiomer being adsorbed preferentially. Although (*S*)-**PCC-67** preferentially recognized and adsorbed the (*R*)-enantiomer of PED molecules from the solution as well, a lower capacity of ∼37% and limited enantioselectivity of ∼19% were observed under identical conditions (Figure 2a).

We assume that the hierarchical pores in (*S*)-**PCC-60** provide more accessible recognition sites for binding chiral substrates, leading to enhanced enantioselective adsorption. In other words, the hierarchical pores of (*S*)-**PCC-60** fully expose interior recognition sites, while the sites are buried in the crystal of (*S*)-**PCC-67**. The differences in adsorption capacity and enantiomeric selectivity of the two adsorbents became more evident when the PED was replaced by bulky substrates such as 3-phenoxypropane-1,2-diol (PPD) and 3-(naphthalen-2-yloxy)propane-1,2-diol (2-NPD). (*S*)-**PCC-60** can still adsorb ∼40% of PPD and ∼36% of 2-NPD, giving the corresponding diols with ∼33% ee and ∼23% ee, respectively (Figure 2d,f). Whereas (*S*)-**PCC-67** only can adsorb ∼3% of PPD and ∼4% of 2-NPD, and its enantioselectivity seems

https://doi.org/10.1021/acscentsci.1c01571
ACS Cent. Sci. 2022, 8, 562−570

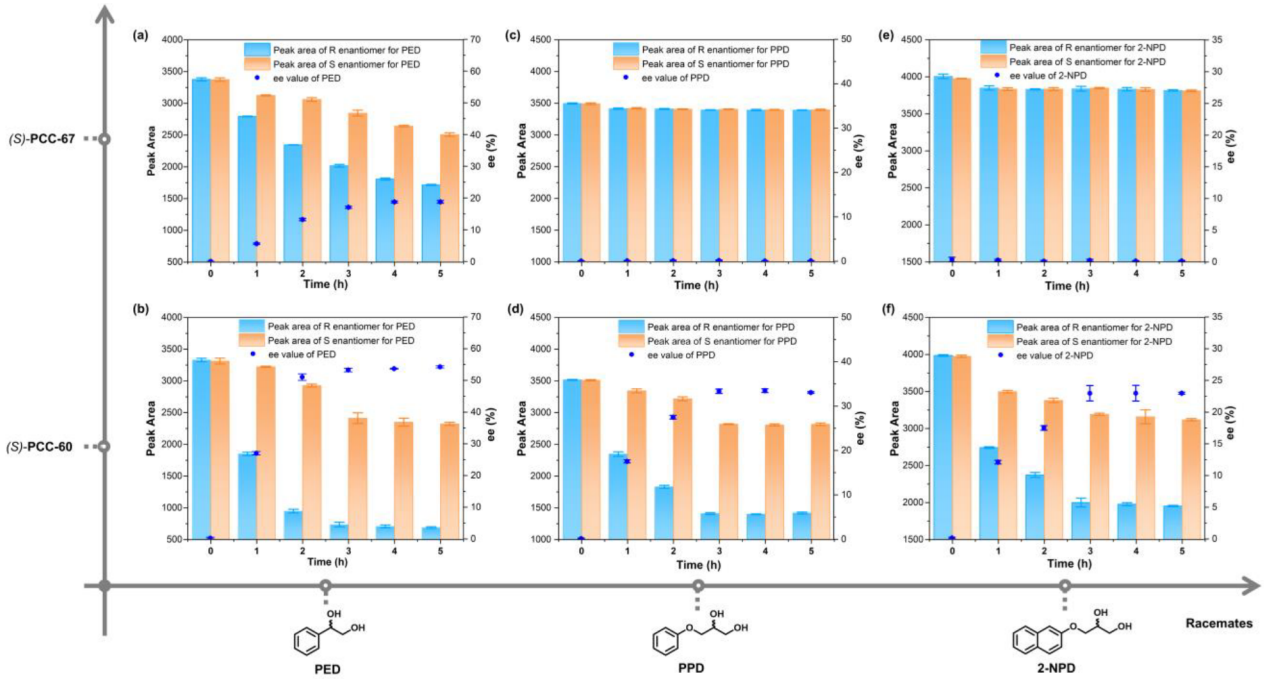

Figure 2. Enantioseparation of racemic diols using (*S*)-**PCC-60** and (*S*)-**PCC-67** with contact times in terms of ee value and enantiomeric peak areas. (a) **PCC-67**/PED, (b) **PCC-60**/PED, (c) **PCC-67**/PPD, (d) **PCC-60**/PPD, (e) **PCC-67**/2-NPD, (f) **PCC-60**/2-NPD.

negligible as well (Figure 2c,e). Perhaps only surface adsorption occurred in (*S*)-**PCC-67**, as its narrow channels exclude the two larger diol molecules. Therefore, the different porosities of **PCC-60** and **PCC-67** significantly affect their enantiosorption performances. The (*S*)-**PCC-60** is assembled from microporous cages interconnected by extrinsic spindle-like mesopores, whereas (*S*)-**PCC-67** is a superstructure with densely packed cages, precluding the mass transfer of chiral substrates. Furthermore, multiple recognition sites in (*S*)-**PCC-60**, including amino acid residues and metal nodes, are decorated on the interior and exterior walls of coordination cages, which are highly accessible for guest molecules. As a result, the hierarchically porous (*S*)-**PCC-60** provides an infinite array of recognition sites within the crystal, leading to excellent enantioselectivity and capacity toward chiral diols. Conversely, most of the recognition sites in (*S*)-**PCC-67** are buried in the narrow pores. The four windows in the cage are blocked by the walls from surrounding cages, limiting their adsorption and selectivity toward chiral diols. Overall, **PCC-60** is a novel hierarchically porous superstructure with accessible chiral sites for potential enantioseparation. To further confirm the presence of hierarchical pores, the dynamic adsorption of **PCC-60** and **PCC-67** toward different guest molecules, including iodine (I_2), 4-nitrophenol (NP), methyl orange (MO), and rhodamine B (Rh B), have been investigated at the same concentration (Figure S12). It was found that **PCC-60** and **PCC-67** showed similar adsorption behaviors for the small molecule I_2. For the NP featuring a similar size to the PED molecule, **PCC-60** exhibits faster adsorption and higher capacity compared to **PCC-67**. Even for bulkier dye molecules, such as MO and RhB, the **PCC-60** crystals still feature a high adsorption capacity. A color change was observed in the crystals after 6 h, whereas **PCC-67** showed no adsorption, indicating that the limited pore sizes of **PCC-67** hindered the ingress of dye molecules (Figures S13 and S14). The adsorption experiments further confirm the presence of channels and cavities of different sizes in the two cage assemblies. The existence of large cavities in **PCC-60** can significantly facilitate the mass transfer and substrate encapsulation in the cage assembly.

Next, the substrate scope of the chiral adsorbent of (*S*)-**PCC-60** was tested with various aromatic diols featuring different electronic properties under the optimized separation condition (Figure 3). First, the PPD analogues with electron-

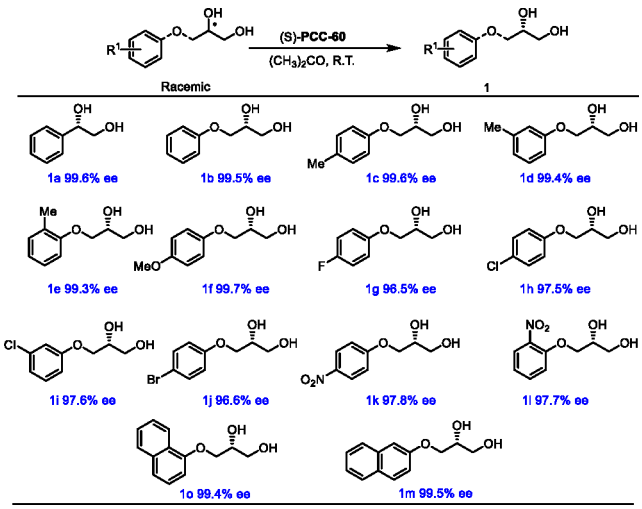

Figure 3. Enantioseparation of racemic 1-phenylethane-1,2-diols and analogues by (*S*)-**PCC-60**.

rich groups, such as methyl and methoxy, on the aromatic ring gave rise to excellent enantioselectivities with ee values up to 99.7% (**1b**−**1f**) (Figure S7). Second, after introducing electron-deficient substituents, such as -F, -Cl, -Br, or -NO_2, to the aromatic ring, the chiral diols could also be resolved by the adsorbent (*S*)-**PCC-60**, affording ee values ranging from

https://doi.org/10.1021/acscentsci.1c01571
ACS Cent. Sci. 2022, 8, 562−570

96.5 to 97.8% (**1g−1l**). Finally, the aromatic diols with steric hindrance, including 3-(naphthalen-1-yloxy)propane-1,2-diol and 3-(naphthalen-2-yloxy)propane-1,2-diol (2-NPD) (**1o−1m**), were also examined for the resolution, giving ee values of 99.4% and 99.5%, respectively. These results indicate that the **PCC-60** features excellent enantioselectivity toward a wide range of chiral diols, representing one of the best coordination compounds for diol enantioseparation.[53−55]

Chiral amines and their derivatives are crucial intermediates in synthesizing numerous drug molecules and natural compounds.[56−58] As such, the performance of (*S*)-**PCC-60** was also investigated by amine enantioseparation. With 1-phenylethylamine (1-PEA) as a model amine, unfortunately, the encapsulated 1-PEA molecules failed to be desorbed from the (*S*)-**PCC-60** owing to their strong interactions. Therefore, the separation was not successful. Despite this, it was found that the supernatant of 1-PEA exhibited a moderate ee value, indicating that (*S*)-**PCC-60** can selectively adsorb (*R*)-enantiomers of 1-PEA. Herein, racemic 1-PEA was acylated with benzoyl chloride to reduce its polarity for ease of desorption. As a result, racemic 1-PEA (**2a**) can be successfully separated by (*S*)-**PCC-60** after benzoylation with excellent enantioselectivity of 99.9% under the optimized conditions (Figure S10). The substrate scope could be extended to other acylated aromatic amines, such as 4-Me-, 4-MeO-, 3-MeO-, 4-F-, or 4-Br-substituted 1-PEA, 1-naphthalen-1-yl-ethylamine (1-NEA), and indan-1-ylamine (**2b−2h**) (Figure 4). In these

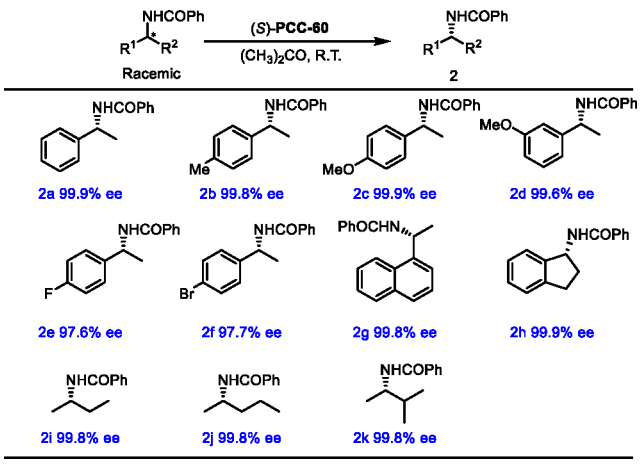

Figure 4. Enantioseparation of racemic benzoylated 1-phenylethylamine and its analogues by (*S*)-**PCC-60**.

resolution processes, **PCC-60** also exhibits superb enantioselectivity with the ee values up to 99.9%. Besides, alkyl amines, compounds more intricate for separation compared with aromatic amines, were tested for resolution. Encouragingly, the small molecular alkyl amines, such as 2-butylamine (**2i**), 2-pentylamine (**2j**), and 3-methyl-2butylamine (**2k**), gave rise to the enantioselectivity of 99.8% ee after benzoylation. These results further demonstrated the versatility of **PCC-60** as a chiral adsorbent. In contrast, the microporous cage assembly, (*S*)-**PCC-67**, was employed as a chiral adsorbent under identical separation conditions, which indicate 24%, 10%, and 10% ee for the small substrates **2i**, **2j**, and **2k**, respectively. Besides, the **PCC-67** failed to separate large substrate **2a**. The control experiments further confirmed the importance of hierarchical porosity in the enantioseparation of cage-based materials.

Moreover, the recycling capability of this solid adsorbent was evaluated by the consecutive resolution of chiral PED and benzoylated 1-PEA. The single crystals of (*S*)-**PCC-60** can be readily recycled through filtration and washing. After being thoroughly exchanged with acetone, the adsorbent will be reused for the subsequent separation. The results of enantioseparation indicated that the recovered sample of (*S*)-**PCC-60** maintained high enantioselectivity toward chiral PED and benzoylated 1-PEA, affording the (*R*)-enantiomer of PED with 99.6%, 99.4%, 99.3%, 99.5%, and 99.4% ee for the runs 1−5, respectively, and the (*R*)-enantiomer of benzoylated 1-PEA with 99.9%, 99.6%, 99.6%, 99.6%, and 99.9% ee for the runs 1−5 (Figures S7 and S10). Besides, PXRD indicated that the adsorbent (*S*)-**PCC-60** retained its crystallinity after the consecutive separation experiments (Figure S2). Moreover, the enantioseparation performance of **PCC-60** was studied after heating the crystals at temperatures varying from 50 to 200 °C, demonstrating that its enantioselectivity toward PED molecules would decrease gradually from 95% to 0% (Figure S7). The removal of guest solvents leads to the integral structural collapse and crystallinity loss at a high temperature (Figure S2).

HPLC Enantioseparation. Inspired by these excellent enantioseparation results, we prepared an HPLC column to explore the practical potential of (*S*)-**PCC-60** as a chiral stationary phase (CSP). The chromatographic technique is powerful and efficient in separating enantiomers.[59−62] For this purpose, an empty stainless-steel column (25.0 cm long ×4.6 mm i.d.) was packed with 4.5 g (*S*)-**PCC-60** crystals under 50 MPa. Before chromatographic separation, the column was conditioned with hexane/isopropanol (IPA) (9:1, v/v) at a flow rate of 0.1 mL/min for 5 h. Then, the performance of the CSP was first evaluated by enantioseparation of a racemic diol, PPD. As expected, the racemate of PPD was successfully resolved and baseline separated on the CSP with hexane/IPA (optimized v/v = 98:2) as the mobile phase at a flow rate of 0.1 mL·min^{-1} at room temperature with UV detection at 254 nm (Figure 5a). The high-resolution enantioseparation with a good selectivity factor (α = 1.11) and chromatographic resolution (R_s = 1.69) was achieved within 25 min. The

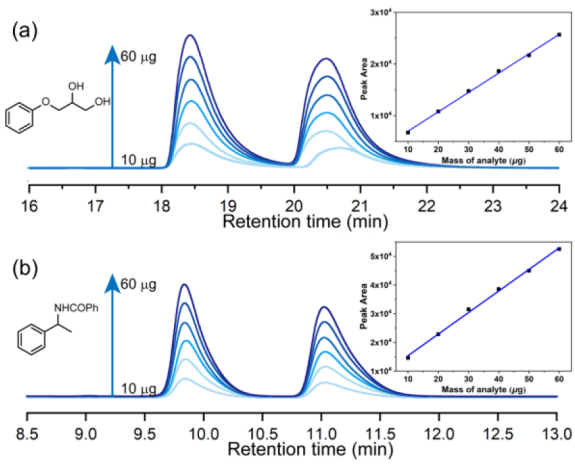

Figure 5. HPLC enantioseparation results based on the (*S*)-**PCC-60**-packed chiral column (25.0 cm long × 4.6 mm i.d.) for (a) PPD racemates, (b) benzoylated 1-PEA racemates. Various injected masses (10 μg, 20 μg, 30 μg, 40 μg, 50 μg, 60 μg) were tested for the separation.

https://doi.org/10.1021/acscentsci.1c01571
ACS Cent. Sci. 2022, 8, 562−570

enantiopure (*S*)-PPD was obtained out of the column first, followed by the (*R*)-PPD, attributed to the stronger interaction of (*R*)-PPD with (*S*)-**PCC-60**. Notably, separation efficiencies as high as 20 490 and 15 644 plates per meter were achieved for (*S*)-PPD and (*R*)-PPD, respectively, confirming the excellent efficiency of the (*S*)-**PCC-60**-based HPLC.

Similarly, racemic 3-(4-methylphenoxy)propane-1,2-diol (4-Me-PPD) and 3-(4-fluorophenoxy)propane-1,2-diol (4-F-PPD) were completely resolved on the (*S*)-**PCC-60** CSP under the identical separation conditions with α/R_s = 1.20/1.77 and 1.17/1.72, respectively (Figure S11). For the bulky diol, 2-NPD, the (*S*)-**PCC-60** column also yielded a good α/R_s value of 1.39/1.88 when using less polar hexane/IPA (v/v = 99:1) as the mobile phase at a flow rate of 0.1 mL·min^{-1} (Figure S11). Furthermore, benzoylated 1-PEA and 1-NEA can also be completely separated with hexane/IPA (v/v = 95:5) as the mobile phase at a flow rate of 0.2 mL·min^{-1}, affording excellent α/R_s of 1.16/1.91 and 1.33/2.87, respectively (Figures 5b and S11). It should be noted that the (*S*)-**PCC-60**-based HPLC column achieved 30 816 and 24 960 plates per meter for (*R*)- and (*S*)-benzoylated 1-PEA, respectively. Remarkably, after one month of shelf life, the (*S*)-**PCC-60** column still maintained excellent performance in the enantiomeric separation toward racemic PPD and benzoylated 1-PEA, yielding α/R_s values of 1.09/1.63 and 1.15/1.70 (Figure S11). In addition, the PXRD pattern of the recovered (*S*)-**PCC-60** CSP was consistent with one of the pristine crystals, indicating its retained crystallinity, despite a slight structural distortion (Figure S2).

What is more, the dye adsorption experiment showed that the recovered (*S*)-**PCC-60** crystals enabled adsorbing 2.69 MO molecules per formula unit, demonstrating the accessible porosity of a cage-based superstructure after HPLC separations (Figure S6). Besides, the recovered (*S*)-**PCC-60** CSP still enabled separating PED with a 97.5% ee, further confirming its durability in the practical enantioseparation (Figure S7). In general, these results indicated the utility of (*S*)-**PCC-60** as a CSP for HPLC. To our knowledge, the **PCC-60** is the first cage-based superstructure that can be directly used as a CSP of efficient HPLC separation. In contrast, the (*S*)-**PCC-67**-based column failed to separate the enantiomers of PPD and benzoylated 1-PEA under similar conditions. Therefore, the hierarchically porous structure of **PCC-60** also plays a significant role in the HPLC separation.

Subsequently, the tolerating capability of (*S*)-**PCC-60** CSP was examined without compromising its resolution. A loading test was conducted using different injection masses. As shown in Figure 5, even when the loading was increased from 10.0 to 60.0 μg for each racemate, PPD or benzoylated 1-PEA can still achieve a baseline resolution under their optimized separation conditions. Such a remarkably high loading makes the (*S*)-**PCC-60** CSP a promising candidate for preparative chromatography. Besides, according to the HPLC results, the chromatographic peak area of every single antipode for the analytes rises linearly with the increase of the injected mass, showing the consistency of the data. Notably, with the increasing injected masses, the theoretical plate number of the (*S*)-**PCC-60**-based HPLC column always remained constant for a specific analyte, indicating that the hierarchical porosity would facilitate the mass transfer of analytes and improve the separation efficiency as a result. It is also noticed that the difference in the retention time for the PPD enantiomer becomes smaller with the increase of injection mass, although achieving baseline resolution. This result may arise from strong hydrogen bonding interactions between hydroxyl groups of PPD and amide groups of **PCC-60**.[63]

■ CONCLUSIONS

In summary, a hierarchically porous assembly **PCC-60** is formed using homochiral lanthanide coordination cages. Its hierarchical porosity originates from a sophisticated arrangement of porous cages, resulting in intrinsic microporous cavities connected by mesopores. Comparing **PCC-60** to an analogue assembly, **PCC-67**, with uniform micropores provides insights into the role of the hierarchical pores. Control experiments confirm that the hierarchical porosity significantly facilitates the mass transfer and access to recognition sites for chiral substrates, conferring high enantioselectivity and a broad substrate scope on the material. Through quantitative studies, the **PCC-60** features excellent enantioselectivity toward diverse significant pharmaceutical intermediates, such as racemic diols and amides. To our knowledge, the **PCC-60** represents the first cage-based assemblies functioning as the chiral stationary phase for HPLC separation, which further confirms the high enantioselectivity, stability, and separation efficiency of this solid adsorbent. Our work not only presents a rare case to assemble homochiral cage-based superstructures with diverse crystal arrangement and pore environments but also unveils the traditionally underestimated role of hierarchical porosity in enantioseparation using porous superstructures. The structural tunability of PCCs, along with the largely untapped hierarchical porosity in cage-based superstructures, brings a bright prospect for constructing an ever-expanding array of efficient enantioseparation materials.

■ ASSOCIATED CONTENT

Supporting Information

The Supporting Information is available free of charge at https://pubs.acs.org/doi/10.1021/acscentsci.1c01571.

Experimental procedures and characterization data (PDF)

Accession Codes

CCDC 2095772 and 2095732 contain the supplementary crystallographic data for this paper. These data can be obtained free of charge via www.ccdc.cam.ac.uk/data_request/cif.

■ AUTHOR INFORMATION

Corresponding Authors

Chengfeng Zhu − *Anhui Province Key Laboratory of Advanced Catalytic Materials and Reaction Engineering, School of Chemistry and Chemical Engineering, Hefei University of Technology, Hefei 230009, P. R. China*; Email: ZhuCF@hfut.edu

Yougui Li − *Anhui Province Key Laboratory of Advanced Catalytic Materials and Reaction Engineering, School of Chemistry and Chemical Engineering, Hefei University of Technology, Hefei 230009, P. R. China*; Email: liyg@hfut.edu

Kun-Yu Wang − *Department of Chemistry, Texas A&M University, College Station, Texas 77843-3255, United States*; orcid.org/0000-0001-8982-0547; Email: wangkunyu@tamu.edu

Hong-Cai Zhou − *Department of Chemistry, Texas A&M University, College Station, Texas 77843-3255, United*

States; Department of Materials Science and Engineering, Texas A&M University, College Station, Texas 77843-3003, United States; orcid.org/0000-0002-9029-3788; Email: zhou@chem.tamu.edu

Authors

Keke Yang − *Anhui Province Key Laboratory of Advanced Catalytic Materials and Reaction Engineering, School of Chemistry and Chemical Engineering, Hefei University of Technology, Hefei 230009, P. R. China*

Hongzhao Wang − *Anhui Province Key Laboratory of Advanced Catalytic Materials and Reaction Engineering, School of Chemistry and Chemical Engineering, Hefei University of Technology, Hefei 230009, P. R. China*

Yu Fang − *State Key Laboratory for Chemo/Bio-Sensing and Chemometrics, College of Chemistry and Chemical Engineering, Hunan University, Changsha, Hunan 410082, P. R. China;* orcid.org/0000-0001-6911-4047

Liang Feng − *Department of Chemistry, Texas A&M University, College Station, Texas 77843-3255, United States*

Jiaqi Zhang − *Department of Chemistry, Texas A&M University, College Station, Texas 77843-3255, United States*

Zhifeng Xiao − *Department of Chemistry, Texas A&M University, College Station, Texas 77843-3255, United States*

Xiang Wu − *Anhui Province Key Laboratory of Advanced Catalytic Materials and Reaction Engineering, School of Chemistry and Chemical Engineering, Hefei University of Technology, Hefei 230009, P. R. China*

Yanming Fu − *Anhui Province Key Laboratory of Advanced Catalytic Materials and Reaction Engineering, School of Chemistry and Chemical Engineering, Hefei University of Technology, Hefei 230009, P. R. China*

Wencheng Zhang − *Anhui Province Key Laboratory of Advanced Catalytic Materials and Reaction Engineering, School of Chemistry and Chemical Engineering, Hefei University of Technology, Hefei 230009, P. R. China*

Complete contact information is available at: https://pubs.acs.org/10.1021/acscentsci.1c01571

Author Contributions

#K.Y., H.W., and Y.F. contributed equally. C.Z. led the project and cowrote the manuscript with Y.L., K.-Y.W., and H.-C.Z. K.Y., H.W., and J. Z. performed the synthesis and separation experiments. Y.F. contributed to the crystal structure analysis. L.F. and K.-Y.W. contributed to the data interpretation of the work and revised it for intellectual content. X.W. and Y.F. performed HPLC column preparation. W.Z. and Z.X. assisted in material characterization and data analysis.

Notes

The authors declare no competing financial interest.

ACKNOWLEDGMENTS

This work was supported by the Fundamental Research Funds for the Central Universities of China (Nos. PA2021GDPK0067, PA2020GDKC0011). The authors appreciate the assistance of the staff from the BL17B beamline of NFPS at the Shanghai Synchrotron Radiation Facility during crystal data collection. We also acknowledge the support of the Robert A. Welch Foundation through a Welch Endowed Chair to H.-C.Z. (A-0030) and the Qatar National Research Fund under Award No. NPRP9-377-1-080.

REFERENCES

(1) Nguyen, L. A.; He, H.; Pham-Huy, C. Chiral Drugs: An Overview. *Int. J. Biomed. Sci.: IJBS* **2006**, *2* (2), 85.

(2) Jiang, W.; Fang, B. Synthesizing Chiral Drug Intermediates by Biocatalysis. *Appl. Biochem. Biotechnol.* **2020**, *192* (1), 146.

(3) Patel, R. N. Biocatalytic Synthesis of Chiral Alcohols and Amino Acids for Development of Pharmaceuticals. *Biomolecules* **2013**, *3* (4), 741.

(4) McConathy, J.; Owens, M. J. Stereochemistry in Drug Action. *Prim. Care Companion J. Clin. Psychiatry* **2003**, *5* (2), 70.

(5) Liu, J.; Mukherjee, S.; Wang, F.; Fischer, R. A.; Zhang, J. Homochiral Metal−Organic Frameworks for Enantioseparation. *Chem. Soc. Rev.* **2021**, *50* (9), 5706.

(6) Dong, J.; Liu, Y.; Cui, Y. Supramolecular Chirality in Metal−Organic Complexes. *Acc. Chem. Res.* **2021**, *54* (1), 194.

(7) Sun, Z.; Hou, J.; Li, L.; Tang, Z. Nanoporous Materials for Chiral Resolution. *Coord. Chem. Rev.* **2020**, *425*, 213481.

(8) Zhang, Y.; Jin, X.; Ma, X.; Wang, Y. Chiral Porous Organic Frameworks and Their Application in Enantioseparation. *Anal. Methods* **2021**, *13* (1), 8.

(9) Han, Z.; Shi, W.; Cheng, P. Synthetic Strategies for Chiral Metal-Organic Frameworks. *Chin. Chem. Lett.* **2018**, *29* (6), 819.

(10) Han, Z.; Wang, K.; Guo, Y.; Chen, W.; Zhang, J.; Zhang, X.; Siligardi, G.; Yang, S.; Zhou, Z.; Sun, P.; Shi, W.; Cheng, P. Cation-Induced Chirality in a Bifunctional Metal-Organic Framework for Quantitative Enantioselective Recognition. *Nat. Commun.* **2019**, *10* (1), 5117.

(11) Chen, X.-Y.; Chen, H.; Đorđević, L.; Guo, Q.-H.; Wu, H.; Wang, Y.; Zhang, L.; Jiao, Y.; Cai, K.; Chen, H.; et al. Selective Photodimerization in a Cyclodextrin Metal−Organic Framework. *J. Am. Chem. Soc.* **2021**, *143* (24), 9129.

(12) Wu, S.; Min, H.; Shi, W.; Cheng, P. Multicenter Metal−Organic Framework-Based Ratiometric Fluorescent Sensors. *Adv. Mater.* **2020**, *32* (3), 1805871.

(13) Zhang, S.-Y.; Yang, C.-X.; Shi, W.; Yan, X.-P.; Cheng, P.; Wojtas, L.; Zaworotko, M. J. A Chiral Metal-Organic Material that Enables Enantiomeric Identification and Purification. *Chem.* **2017**, *3* (2), 281.

(14) Zhang, D.; Ronson, T. K.; Zou, Y.-Q.; Nitschke, J. R. Metal−Organic Cages for Molecular Separations. *Nat. Rev. Chem.* **2021**, *5* (3), 168.

(15) Percástegui, E. G.; Ronson, T. K.; Nitschke, J. R. Design and Applications of Water-Soluble Coordination Cages. *Chem. Rev.* **2020**, *120* (24), 13480.

(16) El-Sayed, E.-S. M.; Yuan, D. Metal-Organic Cages (MOCs): From Discrete to Cage-based Extended Architectures. *Chem. Lett.* **2020**, *49* (1), 28.

(17) Fujita, M.; Tominaga, M.; Hori, A.; Therrien, B. Coordination Assemblies from a Pd(II)-Cornered Square Complex. *Acc. Chem. Res.* **2005**, *38* (4), 369.

(18) Seidel, S. R.; Stang, P. J. High-Symmetry Coordination Cages via Self-Assembly. *Acc. Chem. Res.* **2002**, *35* (11), 972.

(19) Zhang, D.; Ronson, T. K.; Nitschke, J. R. Functional Capsules via Subcomponent Self-Assembly. *Acc. Chem. Res.* **2018**, *51* (10), 2423.

(20) Gosselin, A. J.; Rowland, C. A.; Bloch, E. D. Permanently Microporous Metal−Organic Polyhedra. *Chem. Rev.* **2020**, *120* (16), 8987.

(21) Ueda, Y.; Ito, H.; Fujita, D.; Fujita, M. Permeable Self-Assembled Molecular Containers for Catalyst Isolation Enabling Two-Step Cascade Reactions. *J. Am. Chem. Soc.* **2017**, *139* (17), 6090.

(22) Pan, M.; Wu, K.; Zhang, J.-H.; Su, C.-Y. Chiral Metal−Organic Cages/Containers (MOCs): From Structural and Stereochemical Design to Applications. *Coord. Chem. Rev.* **2019**, *378*, 333.

(23) Tan, C.; Chu, D.; Tang, X.; Liu, Y.; Xuan, W.; Cui, Y. Supramolecular Coordination Cages for Asymmetric Catalysis. *Chem.—Eur. J.* **2019**, *25* (3), 662.

(24) Li, X.; Wu, J.; He, C.; Meng, Q.; Duan, C. Asymmetric Catalysis within the Chiral Confined Space of Metal−Organic Architectures. *Small* **2019**, *15* (32), 1804770.
(25) Ye, Y.; Cook, T. R.; Wang, S.-P.; Wu, J.; Li, S.; Stang, P. J. Self-Assembly of Chiral Metallacycles and Metallacages from a Directionally Adaptable BINOL-Derived Donor. *J. Am. Chem. Soc.* **2015**, *137* (37), 11896.
(26) Fiedler, D.; Leung, D. H.; Bergman, R. G.; Raymond, K. N. Enantioselective Guest Binding and Dynamic Resolution of Cationic Ruthenium Complexes by a Chiral Metal−Ligand Assembly. *J. Am. Chem. Soc.* **2004**, *126* (12), 3674.
(27) García-Simón, C.; Gramage-Doria, R.; Raoufmoghaddam, S.; Parella, T.; Costas, M.; Ribas, X.; Reek, J. N. H. Enantioselective Hydroformylation by a Rh-Catalyst Entrapped in a Supramolecular Metallocage. *J. Am. Chem. Soc.* **2015**, *137* (7), 2680.
(28) Zhang, L.; Liu, H.; Yuan, G.; Han, Y.-F. Chiral Coordination Metallacycles/Metallacages for Enantioselective Recognition And Separation. *Chin. J. Chem.* **2021**, *39*, 2273.
(29) Schulte, T. R.; Holstein, J. J.; Clever, G. H. Chiral Self-Discrimination and Guest Recognition in Helicene-Based Coordination Cages. *Angew. Chem., Int. Ed.* **2019**, *58* (17), 5562.
(30) Howlader, P.; Zangrando, E.; Mukherjee, P. S. Self-Assembly of Enantiopure Pd_{12} Tetrahedral Homochiral Nanocages with Tetrazole Linkers and Chiral Recognition. *J. Am. Chem. Soc.* **2020**, *142* (19), 9070.
(31) Liu, T.; Liu, Y.; Xuan, W.; Cui, Y. Chiral Nanoscale Metal−Organic Tetrahedral Cages: Diastereoselective Self-Assembly and Enantioselective Separation. *Angew. Chem., Int. Ed.* **2010**, *49* (24), 4121.
(32) Hou, Y.-J.; Wu, K.; Wei, Z.-W.; Li, K.; Lu, Y.-L.; Zhu, C.-Y.; Wang, J.-S.; Pan, M.; Jiang, J.-J.; Li, G.-Q.; Su, C. Y. Design and Enantioresolution of Homochiral Fe(II)−Pd(II) Coordination Cages from Stereolabile Metalloligands: Stereochemical Stability and Enantioselective Separation. *J. Am. Chem. Soc.* **2018**, *140* (51), 18183.
(33) Boer, S. A.; White, K. F.; Slater, B.; Emerson, A. J.; Knowles, G. P.; Donald, W. A.; Thornton, A. W.; Ladewig, B. P.; Bell, T. D. M.; Hill, M. R.; Chaffee, A. L.; Abrahams, B. F.; Turner, D. R. A Multifunctional, Charge-Neutral, Chiral Octahedral $M_{12}L_{12}$ Cage. *Chem.—Eur. J.* **2019**, *25* (36), 8489.
(34) Rajasekar, P.; Pandey, S.; Ferrara, J. D.; Del Campo, M.; Le Magueres, P.; Boomishankar, R. Chiral Separation of Styrene Oxides Supported by Enantiomeric Tetrahedral Neutral Pd(II) Cages. *Inorg. Chem.* **2019**, *58* (22), 15017.
(35) Wu, K.; Li, K.; Hou, Y.-J.; Pan, M.; Zhang, L.-Y.; Chen, L.; Su, C.-Y. Homochiral D_4-symmetric Metal−Organic Cages from Stereogenic Ru(II) Metalloligands for Effective Enantioseparation of Atropisomeric Molecules. *Nat. Commun.* **2016**, *7*, 10487.
(36) Zhang, J.-H.; Xie, S.-M.; Zi, M.; Yuan, L.-M. Recent Advances of Application of Porous Molecular Cages for Enantioselective Recognition and Separation. *J. Sep. Sci.* **2020**, *43* (1), 134.
(37) Ng, K.-Y.; Tu, L.-C.; Wang, Y.-S.; Chan, S. I.; Yu, S. S.-F. Probing the Hydrophobic Pocket of the Active Site in the Particulate Methane Monooxygenase (PMMO) from Methylococcus Capsulatus (Bath) by Variable Stereoselective Alkane Hydroxylation and Olefin Epoxidation. *ChemBioChem.* **2008**, *9* (7), 1116.
(38) Alkema, W. B. L.; Dijkhuis, A.-J.; de Vries, E.; Janssen, D. B. The Role of Hydrophobic Active-Site Residues in Substrate Specificity and Acyl Transfer Activity of Penicillin Acylase. *Eur. J. Biochem.* **2002**, *269* (8), 2093.
(39) Zhou, Y.; Li, H.; Zhu, T.; Gao, T.; Yan, P. A Highly Luminescent Chiral Tetrahedral $Eu_4L_4(L)_4$ Cage: Chirality Induction, Chirality Memory, and Circularly Polarized Luminescence. *J. Am. Chem. Soc.* **2019**, *141* (50), 19634.
(40) Tang, X.; Chu, D.; Gong, W.; Cui, Y.; Liu, Y. Metal-Organic Cages with Missing Linker Defects. *Angew. Chem., Int. Ed.* **2021**, *60* (16), 9099.
(41) Yan, L.-L.; Tan, C.-H.; Zhang, G.-L.; Zhou, L.-P.; Bünzli, J.-C.; Sun, Q.-F. Stereocontrolled Self-Assembly and Self-Sorting of Luminescent Europium Tetrahedral Cages. *J. Am. Chem. Soc.* **2015**, *137* (26), 8550.
(42) Xuan, W.; Zhang, M.; Liu, Y.; Chen, Z.; Cui, Y. A Chiral Quadruple-Stranded Helicate Cage for Enantioselective Recognition and Separation. *J. Am. Chem. Soc.* **2012**, *134* (16), 6904.
(43) Rajasekar, P.; Pandey, S.; Paithankar, H.; Chugh, J.; Steiner, A.; Boomishankar, R. Imido-P(v) Trianion Supported Enantiopure Neutral Tetrahedral Pd(II) Cages. *Chem. Commun.* **2018**, *54* (15), 1873.
(44) Bera, S.; Dey, K.; Pal, T. K.; Halder, A.; Tothadi, S.; Karak, S.; Addicoat, M.; Banerjee, R. Porosity Switching in Polymorphic Porous Organic Cages with Exceptional Chemical Stability. *Angew. Chem., Int. Ed.* **2019**, *58* (13), 4243.
(45) Bera, S.; Basu, A.; Tothadi, S.; Garai, B.; Banerjee, S.; Vanka, K.; Banerjee, R. Odd−Even Alternation in Tautomeric Porous Organic Cages with Exceptional Chemical Stability. *Angew. Chem., Int. Ed.* **2017**, *56* (8), 2123.
(46) Spek, A. Single-Crystal Structure Validation with the Program PLATON. *J. Appl. Crystallogr.* **2003**, *36* (1), 7.
(47) Huang, G.; Liu, M.; Xiong, F.; Meng, G.; Tao, Y.; Wu, Y.; Peng, H.; Chen, F. Chiral Syn-1,3-diol Derivatives via a One-Pot Diastereoselective Carboxylation/ Bromocyclization of Homoallylic Alcohols. *iScience* **2018**, *9*, 513.
(48) Shcherbakova, E. G.; James, T. D.; Anzenbacher, P. High-throughput Assay for Determining Enantiomeric Excess of Chiral Diols, Amino Alcohols, and Amines and for Direct Asymmetric Reaction Screening. *Nat. Protoc.* **2020**, *15* (7), 2203.
(49) Wu, X.; Jiang, J.; Chen, Y. Correlation between Intracellular Cofactor Concentrations and Biocatalytic Efficiency: Coexpression of Diketoreductase and Glucose Dehydrogenase for the Preparation of Chiral Diol for Statin Drugs. *ACS Catal.* **2011**, *1* (12), 1661.
(50) Feng, L.; Yuan, S.; Zhang, L.-L.; Tan, K.; Li, J.-L.; Kirchon, A.; Liu, L.-M.; Zhang, P.; Han, Y.; Chabal, Y. J.; et al. Creating Hierarchical Pores by Controlled Linker Thermolysis in Multivariate Metal−Organic Frameworks. *J. Am. Chem. Soc.* **2018**, *140* (6), 2363.
(51) Kokkonen, P.; Bednar, D.; Pinto, G.; Prokop, Z.; Damborsky, J. Engineering enzyme access tunnels. *Biotechnol. Adv.* **2019**, *37* (6), 107386.
(52) Pravda, L.; Berka, K.; Svobodová Vařeková, R.; Sehnal, D.; Banáš, P.; Laskowski, R. A.; Koča, J.; Otyepka, M. Anatomy of Enzyme Channels. *BMC Bioinform.* **2014**, *15* (1), 379.
(53) Zhuo, C.; Wen, Y.; Hu, S.; Sheng, T.; Fu, R.; Xue, Z.; Zhang, H.; Li, H.; Yuan, J.; Chen, X.; et al. Homochiral Metal−Organic Frameworks with Tunable Nanoscale Channel Array and Their Enantioseparation Performance against Chiral Diols. *Inorg. Chem.* **2017**, *56* (11), 6275.
(54) Liu, B.; Shekhah, O.; Arslan, H. K.; Liu, J.; Wöll, C.; Fischer, R. A. Enantiopure Metal−Organic Framework Thin Films: Oriented SURMOF Growth and Enantioselective Adsorption. *Angew. Chem., Int. Ed.* **2012**, *51* (3), 807.
(55) Vaidhyanathan, R.; Bradshaw, D.; Rebilly, J.-N.; Barrio, J. P.; Gould, J. A.; Berry, N. G.; Rosseinsky, M. J. A Family of Nanoporous Materials Based on an Amino Acid Backbone. *Angew. Chem., Int. Ed.* **2006**, *45* (39), 6495.
(56) Yin, Q.; Shi, Y.; Wang, J.; Zhang, X. Direct Catalytic Asymmetric Synthesis of α-Chiral Primary Amines. *Chem. Soc. Rev.* **2020**, *49* (17), 6141.
(57) Nugent, T. C. *Chiral Amine Synthesis: Methods, Developments and Applications*; John Wiley & Sons, 2010.
(58) Islam, M. R.; Mahdi, J. G.; Bowen, I. D. Pharmacological Importance of Stereochemical Resolution of Enantiomeric Drugs. *Drug Saf.* **1997**, *17* (3), 149.
(59) Nuzhdin, A. L.; Dybtsev, D. N.; Bryliakov, K. P.; Talsi, E. P.; Fedin, V. P. Enantioselective Chromatographic Resolution and One-Pot Synthesis of Enantiomerically Pure Sulfoxides over a Homochiral Zn−Organic Framework. *J. Am. Chem. Soc.* **2007**, *129* (43), 12958.
(60) Jiang, H.; Yang, K.; Zhao, X.; Zhang, W.; Liu, Y.; Jiang, J.; Cui, Y. Highly Stable Zr(IV)-Based Metal−Organic Frameworks for Chiral

Separation in Reversed-Phase Liquid Chromatography. *J. Am. Chem. Soc.* **2021**, *143* (1), 390.
(61) Corella-Ochoa, M. N.; Tapia, J. B.; Rubin, H. N.; Lillo, V.; González-Cobos, J.; Núñez-Rico, J. L.; Balestra, S. R. G.; Almora-Barrios, N.; Lledós, M.; Güell-Bara, A.; et al. Homochiral Metal–Organic Frameworks for Enantioselective Separations in Liquid Chromatography. *J. Am. Chem. Soc.* **2019**, *141* (36), 14306.
(62) Ward, T. J.; Ward, K. D. Chiral Separations: a Review of Current Topics and Trends. *Anal. Chem.* **2012**, *84* (2), 626.
(63) Peng, Y.; Gong, T.; Zhang, K.; Lin, X.; Liu, Y.; Jiang, J.; Cui, Y. Engineering Chiral Porous Metal-Organic Frameworks for Enantioselective Adsorption and Separation. *Nat. Commun.* **2014**, *5*, 4406.

https://doi.org/10.1021/acscentsci.1c01571
ACS Cent. Sci. 2022, 8, 562−570